Proc. Natl. Acad. Sci. USA
Vol. 94, pp. 12649–12654, November 1997
Neurobiology

Deciphering a neural code for vision

CHRISTOPHER PASSAGLIA*†‡, FREDERICK DODGE*†‡, ERIK HERZOG*†§, SCOTT JACKSON†, AND ROBERT BARLOW*‡¶

*Marine Biological Laboratory, Woods Hole, MA 02543; †Department of Bioengineering and Neuroscience, Syracuse University, Syracuse, NY 13244; and ‡Center for Vision Research, Department of Ophthalmology, 3258 Weiskotten Hall, State University of New York Health Science Center, 750 East Adams Street, Syracuse, NY 13210

Edited by John E. Dowling, Harvard University, Cambridge, MA, and approved September 10, 1997 (received for review June 2, 1997)

ABSTRACT **Deciphering the information that eyes, ears, and other sensory organs transmit to the brain is important for understanding the neural basis of behavior. Recordings from single sensory nerve cells have yielded useful insights, but single neurons generally do not mediate behavior; networks of neurons do. Monitoring the activity of all cells in a neural network of a behaving animal, however, is not yet possible. Taking an alternative approach, we used a realistic cell-based model to compute the ensemble of neural activity generated by one sensory organ, the lateral eye of the horseshoe crab, *Limulus polyphemus*. We studied how the neural network of this eye encodes natural scenes by presenting to the model movies recorded with a video camera mounted above the eye of an animal that was exploring its underwater habitat. Model predictions were confirmed by simultaneously recording responses from single optic nerve fibers of the same animal. We report here that the eye transmits to the brain robust "neural images" of objects having the size, contrast, and motion of potential mates. The neural code for such objects is not found in ambiguous messages of individual optic nerve fibers but rather in patterns of coherent activity that extend over small ensembles of nerve fibers and are bound together by stimulus motion. Integrative properties of neurons in the first synaptic layer of the brain appear well suited to detecting the patterns of coherent activity. Neural coding by this relatively simple eye helps explain how horseshoe crabs find mates and may lead to a better understanding of how more complex sensory organs process information.**

Living in a world rich with information, animals are highly efficient at extracting what is essential for their survival. The first stage of visual processing begins in the eye where the retina transforms patterns of incident light intensity into trains of impulses in optic nerve fibers (1). The retina can encode information in a reliable and efficient manner (2, 3) but does not encode all of it. Rather the retina emphasizes certain features in the visual scene at the expense of others, presumably to help animals find food, locate mates, and avoid predators (4–6). Knowing what an animal can see is crucial for exploring the neural code the eye transmits to the brain.

We report here a study of neural coding in the lateral eye of the horseshoe crab, *Limulus polyphemus*. We selected *Limulus* as a model system because its lateral eye contains the largest neural network for which a quantitative cell-based model exists (7–9), and its visually guided behavior is well known (10, 12, 13).

Field studies show that vision has an important role in *Limulus* mating behavior (10). In the spring millions of crabs migrate to the ocean's edge from Maine to Mexico to build nests and deposit eggs (11). Male crabs use their lateral eyes to find mates, whereas females use them to avoid nesting sites of other crabs (10, 12). The crabs can see other horseshoe crabs and objects resembling them under a wide variety of illumination conditions despite large differences in the contrast of their carapace (12, 13). Fig. 1*b* shows underwater photographs of black and gray cylindrical objects that approximate the size and range of contrast of the female carapace. Even though the gray object is much less apparent, male crabs can detect it almost as well as the black one (12, 13).

Such visual performance is remarkable in view of the rather simple design of the animal's lateral eyes. Each compound eye samples the underwater world with ≈1,000 hexagonally packed receptor units (ommatidia). Individual ommatidia collect light from a relatively large region of space (≈6°), giving the animal a nearly hemispheric field of view (14). A cluster of retinular cells within each ommatidium transduces the light into electrical signals that passively propagate into a single spike-firing eccentric cell. By using neural mechanisms generally found in more complex retinas, the eccentric cell converts the signals into a train of action potentials that it transmits to nearby ommatidia and the brain. Detailed studies of the integrative properties of these cells have yielded a quantitative description of the response of an ommatidium in terms of its excitation by light and inhibition from neighboring ommatidia (7, 8, 15, 16, 18).

Our strategy for deciphering the retinal code underlying visually guided behavior of *Limulus* was first to videotape the lateral eye's view of its underwater world with a crab-mounted camera. Second, we recorded simultaneously from the optic nerve fiber of an ommatidium viewing the central region of the videotaped scene. Third, we computed the ensemble of optic nerve activities in response to the video by using a model of the eye. Fourth, if the response computed for the appropriate neuron in the model matched that recorded from the nerve fiber, we examined the array of computed responses for putative coding of behaviorally relevant objects.

MATERIALS AND METHODS

Underwater Video Recording. We recorded underwater movies with a miniature video camera ("CrabCam") attached to the carapace of crabs moving in the shallow waters (<1 m depth) of an estuary (Fig. 1*a*). At the same time, we monitored the activity of an optic nerve fiber from one of their lateral eyes. The optic axis of the CrabCam (72° × 54° field of view; model V-1210, Marshall Electronics, Culver City, CA; model SVS-1, Chinon American, Mountainside, NJ) was 4 cm above the eye and aligned parallel with that of the recorded neuron. Video signals were recorded simultaneously with spike discharges of the nerve fiber on a VHS camcorder. Animals freely explored their surroundings or were moved along an underwater track at a speed of ≈15 cm/s, which is the average velocity of swimming horseshoe crabs (17). They moved past stationary cylindrically shaped black and gray objects that approximate the size and range of contrasts of adult females

The publication costs of this article were defrayed in part by page charge payment. This article must therefore be hereby marked "*advertisement*" in accordance with 18 U.S.C. §1734 solely to indicate this fact.

This paper was submitted directly (Track II) to the *Proceedings* office.
Abbreviation: ips, impulses per second.
§Present address: Center for Biological Rhythms, University of Virginia, Charlottesville, VA 22903.
¶To whom reprint requests should be addressed.

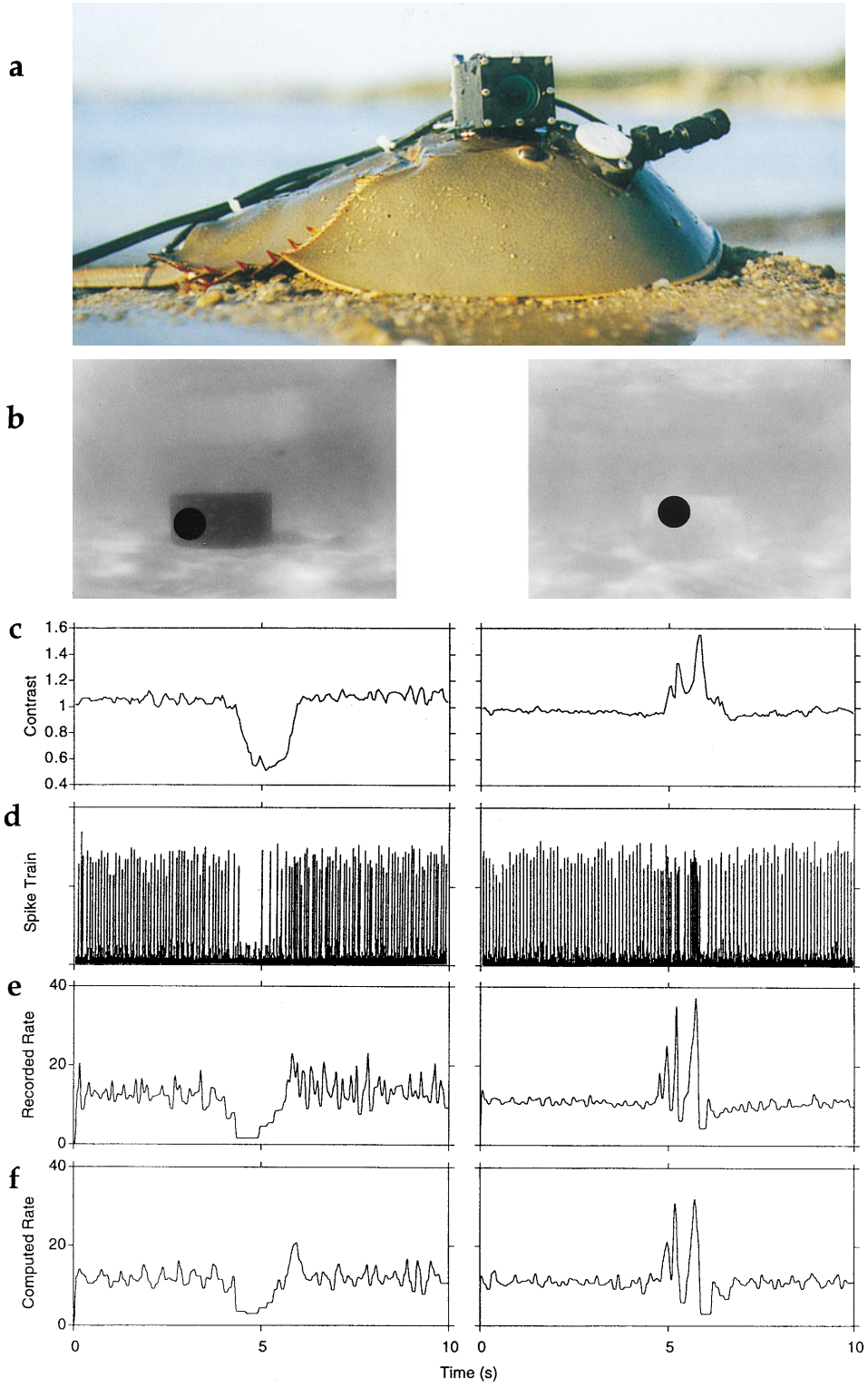

FIG. 1. (*a*) A horseshoe crab, *Limulus polyphemus*, at the water's edge mounted with a video camera, CrabCam, for recording underwater movies and a microsuction electrode for recording responses from a single optic nerve fiber. The barrel of the electrode protrudes to the right from the recording chamber, which is sealed with a white cap (2.5 cm diameter). Cables lead the video and optic nerve signals to recording electronics located on an overhead skiff as the animal moves about underwater at depths of 0.5 to 1 m. (*b*) CrabCam images of a high-contrast black object (*Left*) and a low-contrast gray object (*Right*). Black disks indicate the fields of view of the ommatidia whose optic nerve responses were recorded with the microsuction electrode. (*c*) Light intensities (given as contrast) incident on the recorded ommatidia plotted as a function of time as the animal moved past the black (*Left*) and gray (*Right*) objects. Contrast is the ratio of the intensity of a pixel to the average intensity of the scene. (*d*) Recordings with the microsuction electrode of spike trains from single fibers in response to the 10-s sequences of light intensities shown in *c*. (*e*) Recorded trains of spikes in *d* plotted as instantaneous frequencies, which are the reciprocals of the intervals between nerve impulses. (*f*) Instantaneous frequencies computed by the cell-based model in response to digitized video images of the black and gray objects. The objects passed through the fields of view of the recorded and model neurons from 4 to 6 s after the start of the runs evoking reduced (black object) and quasi-periodic (gray object) responses. Responses are representative of those recorded under similar conditions in other field experiments (n = 53 trials).

(30 cm diameter; 15 cm high). The objects were placed 75 cm away because field studies show that about half of the male crabs detect and turn toward them at this distance (13).

Video sequences (10-s duration) were digitized at 20 frames/s (120 × 160 pixels; 8 bits resolution) by using commercial software (Videofusion, Maumee, OH). We rescaled the digitized movies by using a nonlinear mapping function that inversely corrects for the gamma response characteristic of the video camera and for output saturation (18). We compensated for automatic gain controls of the camera, camcorder, and computer by subtracting from all frames of a movie the black level of a black and white test patch viewed by the CrabCam. The contrast of the black object determined by these procedures matched well that measured from photographs taken underwater with high-latitude TMAX-100 film (Kodak). The turbid, shallow waters where *Limulus* mate reduce the contrast of underwater objects exponentially with distance (attenuation coefficient of $\approx 1.2\ m^{-1}$) such that objects beyond 1.5–2 m are essentially invisible (18).

Optic Nerve Recording. We recorded spike trains of single optic nerve fibers from behaving animals by using a water-tight microsuction electrode (17). Fig. 1*a* shows the recording chamber and electrode attached to the carapace anterior to the right lateral eye. To access the optic nerve, we trephined a hole in the carapace ≈2 cm anterior to the eye, slid the tongue of the saline-filled recording chamber under the nerve trunk, and fastened the chamber to the carapace. The sheath of the nerve was slit open, and a single active fiber was teased free and sucked into the 200 μm electrode tip. The pixel of digitized movies that intercepted the optic axis of the recorded neuron was identified by averaging frames coinciding with nerve impulses in response to a small probe light. Optic nerve signals were led via a cable (15 m length) to an AC amplifier (Electronics Shop, The Rockefeller University, New York) and the audio channel of the camcorder. The audio channel output was digitized off-line at 11 kHz, and the spike firing times (Fig. 1*d*) were converted to instantaneous firing rates and plotted as a function of time (Fig. 1*e*).

Computing Optic Nerve Responses. We computed patterns of spike activity for the ensemble of optic nerve fibers by feeding the CrabCam movies to a realistic cell-based model of the lateral eye. To determine the light intensity incident on each ommatidium of the model, we convolved each frame of a movie with a Gaussian point-spread function that matched the acceptance angle of an ommatidium (6° at half-maximal sensitivity, ref. 19) by using public-domain software (NIH Image Version 1.6), and then we sampled the blurred frames at points of intersection with the optic axes of the array of ommatidia (14). The size of the model was limited to a 12 × 16 array of neurons by the field of view of the CrabCam. Each frame of a movie thus yielded a 12 × 16 array of pixels specifying the relative light intensities incident on each ommatidium at an instant in time (see Fig. 1*c*), and the sequence of frames (Fig. 2*a*) comprised an optically transformed movie of the stimulus to the retina as the animal explored its underwater world.

The movie then was fed to the model, which computed spike trains for the ensemble of optic nerve fibers by using a set of differential equations representing the excitatory properties of each ommatidium and the inhibitory interactions between them. Details of the model are presented elsewhere (18). In brief, incident light intensities were converted into voltage fluctuations (quantum bumps) according to an adapting bump model (20, 21). To account for transduction noise, which contributes 6–10% to the coefficient of variation of fluctuations in instantaneous firing rates in our experiments, quantum bumps were randomly generated by a Poisson process at a rate dependent on light intensity (20) and summed to form the receptor potential by using a four-stage version of the Fuortes–Hodgkin model (22). The receptor potential then was attenuated by the passive cable

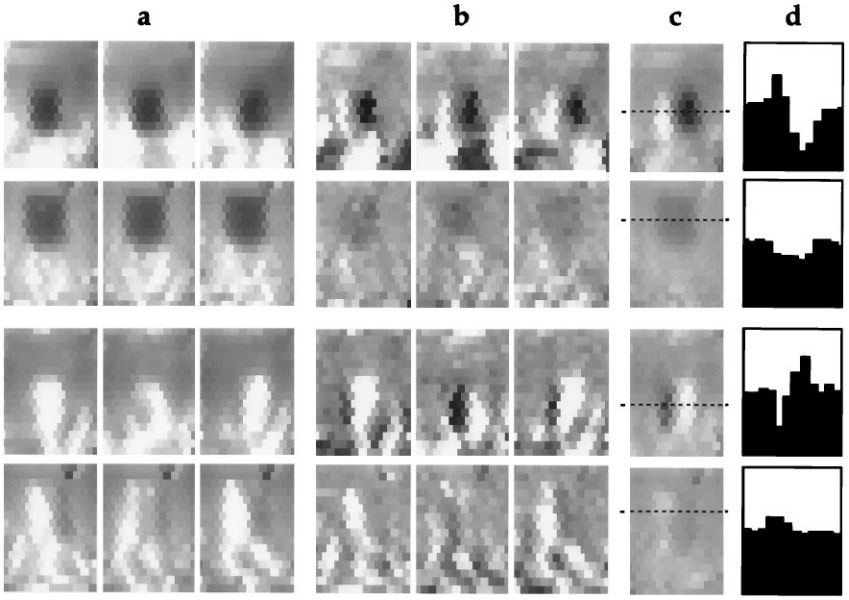

FIG. 2. (*a*) CrabCam images of the black and gray objects after optical sampling. The arrays of pixels show the light intensities incident on the 12 × 16 array of ommatidia viewing the videotaped scene. Rows 1 and 2 show images of the black object while the animal was moving and stationary, respectively. Rows 3 and 4 show corresponding images of the gray object. Interval between displayed sequences is 0.25 s. (*b*) Computed neural images of the optically transformed visual images in *a*. The arrays of pixels give the computed firing rates of optic nerve fibers mapped onto a gray scale with black set to 0 ips and white set to twice the mean firing rate. Mean firing rates to the uniform background illumination in rows 1, 2, 3, and 4 were 12, 20, 13, and 18 ips, respectively. (*c*) Computed neural images of activity in the brain generated by the eye's output in *b*. The arrays of pixels give the simulated responses of brain neurons having integration times of 400 ms mapped onto a gray scale with black set to 0 and white set to twice the mean. Each image sums eight sequential neural images from the eye. Computed images are based on the temporal properties of brain neurons and not their spatial interactions. (*d*) Simulated responses of brain neurons evoked by the activities of an equal number of ommatidia located in a horizontal row of the model eye (dashed lines in *c*). Movies of the underwater video recordings and their computed neural images can be viewed at Center for Vision Research at http://www.hscsyr.edu/~eye.

properties of the eccentric cell and integrated with lateral and self-inhibitory potentials to form the generator potential (23). The lateral inhibitory inputs to an eccentric cell were computed by using a dynamic version of the original Hartline–Ratliff formulation (7, 24) with inhibitory strength weighted as a function of retinal distance (25, 26). The self-inhibitory input to an eccentric cell was calculated by integrating a decaying exponential function triggered by each impulse the cell fired (27). The generator potential was further decremented by a putative electrogenic pump (28, 29) and converted into a train of nerve impulses with a leaky integrate-and-fire encoder at a rate of 1 impulse/mV above a threshold of 1 mV (30). Computed trains of impulses were expressed as instantaneous firing rates for each frame of the movie, converted to a linear gray scale, and mapped back onto two-dimensional arrays of pixels yielding a time series of "neural images" (31), which are snapshots of the eye's input to the brain (Fig. 2*b*).

For all computations we set the 10 parameters of the model to those derived from the average spatiotemporal transfer function of the eye measured in the laboratory (18, 26, 34). For each experiment we scaled two parameters to simulate illumination levels in the field. We trimmed one parameter, the mean bump rate, to match the estimated transduction noise and scaled another, the sensitivity of the spike encoder, to match the mean firing rate of the recorded neuron. We extended these parameters to all ommatidia in the model because previous studies have shown that cells in a given eye have the same properties (15, 25).

The accuracy of the model was checked first by comparing optic nerve responses computed for controlled stimuli with those recorded from single optic nerve fibers in the laboratory, and second by comparing responses computed for underwater movies with those recorded in the field. Optic nerve responses to drifting bars recorded in the laboratory were indistinguishable from those computed with the model, that is, responses recorded to successive presentations of the same stimulus were as correlated with those computed by the model as with each other (18). Correlation coefficients were consistently >0.95 for controlled laboratory experiments ($n = 5$) but were lower (>0.75) for field experiments ($n = 5$) because of difficulties in determining precisely the stimulus to the recorded neuron. All field experiments yielded results similar to those reported here.

Measuring Transfer Functions. We measured the eye's integrative properties by recording the responses of single optic nerve fibers to sinusoidally modulated light of different spatial and temporal frequencies presented to animals submerged in a seawater tank in the laboratory ($n = 8$). Visual stimuli (VENUS, Neuroscientific, New York, NY) were displayed on a monitor (10×13 cm, Tektronics, model 608, Beaverton, OR) placed in front of a glass window on the tank, 4 cm from the eye, and centered on the optic axis of the recorded neuron. Spatial transfer functions were measured by drifting sinewave gratings of different spatial frequencies across the monitor. Temporal transfer functions were measured by modulating a 6° spot of light (field of view of an ommatidium) with the sum of five temporal frequencies chosen to prevent phase locking of spike discharges (32). Response gains were calculated for each of the five frequency components by first estimating the relative modulation of the recorded firing rate by using the method of least squares and then normalizing the result with the contrast of the stimulus.

RESULTS AND DISCUSSION

Responses of Single Optic Nerve Fibers. Fig. 1 *e* and *f* plot the responses recorded from a single optic nerve fiber and computed for the corresponding neuron in the model as an animal moved past high- and low-contrast crab-size objects in the ocean. Computed and recorded responses match qualitatively in amplitude, shape, and noise properties, indicating that the essential features of optic nerve responses are well represented by the model. Note that the variability in firing rate when the black object is outside the recorded receptor's field of view (coefficient of variation ≈ 0.27) is significantly greater than in the case of the gray one (coefficient of variation ≈ 0.1). This results from the field of view (black disk) of one receptor being oriented slightly lower and thus seeing more of the bright flickering light reflected from the sandy bottom. The relative light intensities incident on these receptors can be seen in Fig. 1*c*. Because transduction noise produces $\approx 10\%$ of the variation in a spike train for steady illumination, higher variability results from underwater lighting. Hence, both neural and environmental noise limit the detectability of these behaviorally relevant objects.

The good correspondence between theory and experiment in Fig. 1 not only confirms the accuracy of the model but also reveals an interesting difference in optic nerve responses to high- and low-contrast objects. Note that as the animal moved past the black object the firing rate of the optic nerve fiber initially decreased and then briefly increased (Fig. 1 *e* and *f*, *Left*); whereas, the firing rate to the gray object increased in a quasi-periodic fashion because of flickering light in the underwater scene (Fig. 1 *e* and *f*, *Right*). Although single optic nerve fibers do not respond in the same way to the high- and low-contrast objects in the ocean, male horseshoe crabs detect both objects about equally well.

Responses of Arrays of Optic Nerve Fibers. Clues about how horseshoe crabs detect other horseshoe crabs and objects resembling them (Fig. 1*b*) can be found in the large arrays of optic nerve responses, or neural images, computed by the model eye (Fig. 2*b*). Each pixel of a neural image corresponds to an ommatidium in the eye, and its gray level gives the optic nerve firing rate computed for that ommatidium at an instant in time. Inspection of the neural images in rows 1 and 3 of Fig. 2*b* reveals small clusters of ommatidia responding with transient increases (white pixels) and decreases (black pixels) in firing rate to images of crab-size objects moving across the visual field. Note that the eye encodes both moving high-contrast (row 1) and low-contrast (row 3) objects with a characteristic spatial pattern of optic nerve activity, even though the responses of single nerve fibers to the objects differ (Fig. 1 *d* and *e*). Clusters of ommatidia responding together at high rates (light regions) lie next to clusters responding at low rates (dark regions). In laboratory simulations the light and dark regions merge together for smaller objects and separate for larger ones, reducing the modulation of optic nerve responses in both cases (18). In the lower part of the visual field, flickering light reflected off the sand modulates optic nerve responses partially obscuring those to the crab-size objects.

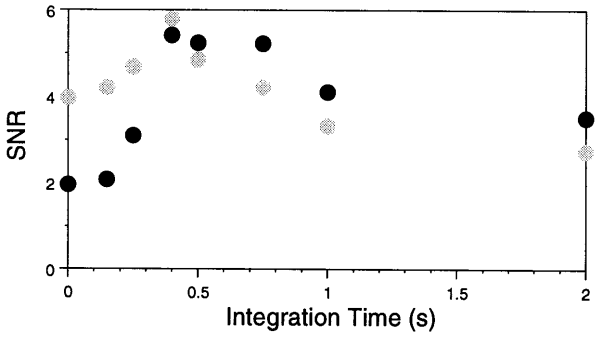

FIG. 3. Temporal integration of optic-nerve responses by neurons in the first synaptic layer of the brain. The gray and black symbols plot the signal-to-noise ratio (SNR) of simulated responses of brain neurons to moving images of the gray and black objects in Fig. 2, respectively, as a function of synaptic integration time. SNR is defined as the peak-to-peak response modulation of neurons viewing the objects relative to twice the standard deviation of response modulations of the rest of the network.

Processing Patterns of Optic Nerve Activity in the Brain. How might neurons in the brain distinguish responses to moving crab-size objects from those evoked by other dynamic stimuli? A possible answer is suggested by a recent finding that central neurons integrate optic nerve signals with synaptic time constants on the order of 300–500 ms (18). Integrating optic nerve responses in Fig. 2*b* with a time constant of 400 ms (average of eight sequential neural images computed every 50 ms) yields neural images of average brain activity in which responses to moving crab-sized objects are enhanced relative to flicker in the foreground (Fig. 2*c*). Profiles of simulated brain activity evoked by a horizontal row of optic nerve fibers reveal a 132% modulation to the moving black object [(18 impulses/s (ips)–3 ips)/12 ips] and an 87% modulation to the moving gray one [(19 ips–8 ips)/13 ips] (Fig. 2*d*). The greater response modulation to the black object may correspond to the field observation that animals can see it slightly better than the gray one (13). Integrating optic nerve responses over periods longer or shorter than 400 ms yields less robust responses to the moving crab-size objects (Fig. 3). An integration time of 400 ms gives maximal signal-to-noise ratio as defined by half of the peak-to-peak modulation of the response to the object divided by the standard deviation of responses to surrounding regions of the scene. Integrative mechanisms in the brain thus appear well suited for sensing moving crab-size objects in the neural images it receives from the eye.

The Importance of Motion. The neural images of stationary objects dramatically illustrate the essential role of motion to retinal coding. Whereas visual images of stationary objects appear similar to those of moving objects (Fig. 2*a*), their neural images do not. The objects are hardly recognizable in the computed neural images of optic nerve activity (Fig. 2*b*) and nearly invisible in the neural images of simulated brain activity (Fig. 2*c*) when they are not moving in the animal's visual field. Indeed, response profiles in Fig. 2*d* reveal an amplitude of modulation of just 27% [(20 ips–14 ips)/20 ips)] for the black object and 22% [(20 ips–16 ips)/18 ips)] for the gray one. Image motion thus produced over a 4-fold increase in gain for the black (132%/27%) and gray (87%/22%) objects.

Seeing High-Contrast Objects. Strongly modulated responses to moving images of high-contrast objects (Fig. 2*b*, row 1) are understandable in terms of the eye's optical and neural properties. Coarse sampling by the ommatidia (14) and lateral inhibitory interactions among them (7) reduce the eye's sensitivity to high and low spatial frequencies, respectively, yielding a broadly tuned spatial filter (26). The eye is maximally sensitive (Fig. 4*a*, shaded region) for spatial frequencies from 0.008 to 0.04 cycles/degree, which correspond to crab-size objects at distances of 0.25 to 1.4 m where 98% of visual detection occurs (13). With regard to the temporal response properties of the eye, the duration of photoreceptor quantal responses to light (22, 33) and the dynamics of self-inhibition (27) reduce its sensitivity to high and low temporal frequencies, respectively, resulting in a tuned temporal filter (26, 34). The eye is highly sensitive to images of crab-size objects moving within the animal's visual range at about the speed of a horseshoe crab (15 cm/s) and up to twice these speeds for animals passing one another in opposite directions (17). These speeds roughly correspond to temporal frequencies from 0.5 to 6 cycles/s for which response gains exceed one (Fig. 4*b*, region shaded with negative slope lines), underscoring the eye's high sensitivity to moving objects. The spatiotemporal properties of the eye can readily account for the animal's ability to see high-contrast objects but not low-contrast ones.

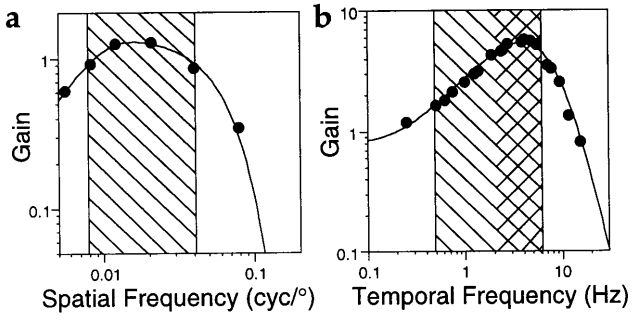

FIG. 4. Spatiotemporal response properties of the lateral eye. (*a*) Spatial transfer function. Gain of the response of a single optic nerve fiber plotted as a function of the spatial frequency of a drifting sinusoidal grating. Negative slope lines denote the frequency band corresponding to crab-size objects at the range of distances which *Limulus* detect potential mates in their natural habitat (0.25–1.4 m). (*b*) Temporal transfer function. Response gain plotted as a function of the frequency of a flickering spot that fills the field of view of the recorded ommatidium. Positive slope lines denote the frequency band corresponding to animal velocities over the range of distances of mate detection (0.5–6 Hz). Negative slope lines give the frequency range of strobic lighting (2–6 Hz) in the animal's natural underwater environment.

Seeing Low-Contrast Objects. Natural fluctuations of underwater lighting enhance the visibility of low-contrast objects (35). Surface waves, acting as dynamic lenses, create beams of light that strobe the underwater scene at frequencies of ≈2–6Hz for which the lateral eye is maximally sensitive (Fig. 4*b*, region shaded with positive slope lines; ref. 36). Such wave-induced flicker is a prominent feature of the shallow waters where *Limulus* mate and persists over a range of lighting conditions (37), which is consistent with the animal's ability to find mates day and night (10–13). Behavioral studies in mating areas show that strobic light increases the probability that male *Limulus* turn toward and approach the low-contrast gray object (38). Model computations show that the strobic light reflects off low-contrast objects, enhancing their neural images as the objects move across the animal's visual field (Fig. 2*b*, compare images in rows 3 and 4). We note that strobic light also evokes coherent bursts of nerve impulses from neighboring ommatidia in the absence of relative motion. How then does relative motion of objects enhance their neural image? Motion of an image across the visual field activates receptors along its path (Fig. 2*b*, row 3, white pixels) leaving

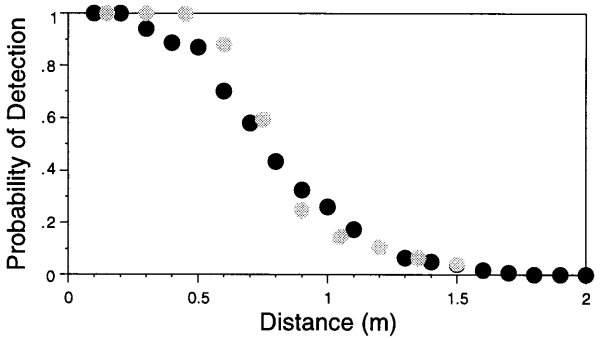

FIG. 5. Comparison of the visual performance of horseshoe crabs to that predicted from the computational model. Black symbols replot from a behavioral study (13) the probability of crabs turning toward a black crab-size object as a function of the distance from the object. Gray symbols plot the visual performance of an ideal horseshoe crab predicted from optic nerve responses computed by the model. We assume that the ideal horseshoe crab moved past the object at an average speed of 15 cm/s and water turbidity decreased the object's contrast with distance (see *Materials and Methods*). We use signal detection theory to estimate the probability of detecting the computed optic nerve responses in the presence of noise. A coefficient of variation of 0.1 in firing rate noise and a threshold for detection permitting a 1% false-alarm rate provided the best description of the measured visual performance. The higher coefficient of variation measured in the field (0.2) suggests that the decision maker in the crab brain pools the activities of a small cluster of optic nerve fibers (≈4), which is consistent with the number of ommatidia viewing the object at behavioral threshold (13, 14). Significantly different estimates of visual performance require at least a 10-fold change in detection threshold or a 2-fold change in noise level.

adapted ones in its wake (Fig. 2*b*, row 3, dark pixels). Without motion of images across its receptor surface, the eye provides no cues for distinguishing flickering light reflected off the object from that reflected off the sand, making these parts of the scene appear continuous (Fig. 2, row 4). In short, no visual cues distinguish object from foreground in the absence of relative motion. Subsequent integration by the brain further enhances the neural images of moving objects (Fig. 2*c*) because the integration time of brain neurons matches the velocity range of horseshoe crabs and not that of the fast-moving flicker. Flicker-induced responses (2–6 Hz) are shorter than the integration time of 400 ms whereas object motion across receptors is longer (≈2 s), yielding a substantial response envelope (Fig. 2 *c* and *d*). Image motion thus binds together the activities of neighboring clusters of ommatidia in space and time, sending robust signals to the brain about potential mates.

CONCLUSION

Adrian and Hartline were the first to study neural coding in single sensory fibers. They reported that the mean firing rate of nerve impulses encoded various elementary features of stimuli to proprioreceptors (39) and visual receptors (40). Later studies in the auditory systems showed that the precise time of occurrence of nerve impulses transmits information about sound frequencies and their location in space (41, 42). Similar claims have been made recently for the visual systems of salamanders and rabbits (43). Such a timing code appears not to have an important role in *Limulus* vision because neurons in the brain integrate over periods of 250–500 ms trains of optic nerve impulses with interspike intervals ranging from 25 to 200 ms (18). As a consequence of strobic underwater lighting, spatiotemporal properties of the eye, and temporal properties of brain cells, objects having the size, contrast, and motion of horseshoe crabs are not distinguished by unique neural codes. Low-pass integrative properties of brain neurons filter out rapid changes, yielding response envelopes that represent coherent changes in the mean firing rates among ommatidia viewing a moving object. Fig. 5 shows that estimates from such a rate code can account reasonably well for the visual performance of horseshoe crabs.

The *Limulus* eye processes visual information with excitatory and inhibitory mechanisms similar to those found in the first synaptic layer, or outer plexiform layer, of the vertebrate retina. Both retinas integrate photoreceptor signals with lateral inhibitory mechanisms, but the vertebrate retina adds a second synaptic layer of processing, the inner plexiform layer, before transmitting optic nerve signals to the brain (1). With two layers of neural processing, the frog's eye, for example, can extract specific features of its visual world such as small, moving dark objects about the size of a fly and transmit information about them to the brain (4, 44). The integrative mechanisms of the *Limulus* eye also extract information about moving objects, encoding those resembling a horseshoe crab with characteristic patterns of coherent activity among clusters of optic nerve fibers. Neurons in the first synaptic layer of the brain integrate optic nerve signals, further enhancing the neural images of potential mates.

We thank A. Meigs, R. Mitchell, A. Wixson, S. Dodge, M.E. Kelly-Manglapus, D. Porcello, L. Sher, E. Kaplan, D. Samber, and M. Powers for their help. This work was supported by the National Institutes of Health (MH 49741 and EY00667) and the National Science Foundation (IBN9696208).

1. Dowling, J. E. (1987) *The Retina: An Approachable Part of the Brain* (Harvard Univ. Press, Cambridge, MA).
2. Rieke, F., Warland, D., DeRuyter van Steveninck, R. R. & Bialek, W. (1997) *Spikes: Exploring the Neural Code* (MIT Press, Cambridge, MA).
3. Bialek, W. & Owen, W. G. (1990) *Biophys. J.* **58,** 1227–1233.
4. Lettvin, Y. L., Maturana, H. R., McColluch, W. S. & Pitts, W. H. (1959) *Proc. Inst. Radio Eng.* **47,** 1940–1951.
5. Levine, J. S. & MacNichol, E. F. (1979) *Sens. Processes* **3,** 95–131.
6. Laughlin, S. B. (1996) *Vision Res.* **36,** 1529–1541.
7. Hartline, H. K. & Ratliff, F. (1957) *J. Gen. Physiol.* **40,** 357–376.
8. Hartline, H. K. & Ratliff, F. (1958) *J. Gen. Physiol.* **41,** 1049–1066.
9. Barlow, R. B., Prakash, R. & Solessio, E. (1993) *Amer. Zool.* **33,** 66–78.
10. Barlow, R. B., Ireland, L. C. & Kass, L. (1982) *Nature (London)* **296,** 65–66.
11. Barlow, R. B., Powers, M. K., Howard, H. & Kass, L. (1986) *Biol. Bull. Woods Hole, Mass.* **171,** 310–329.
12. Powers, M. K., Barlow, R. B. & Kass, L. (1991) *Visual Neurosci.* **7,** 179–189.
13. Herzog, E. D., Powers, M. K. & Barlow, R. B. (1996) *Visual Neurosci.* **13,** 31–41.
14. Herzog, E. D. & Barlow, R. B. (1992) *Visual Neurosci.* **9,** 571–580.
15. Ratliff, F., ed. (1974) *Studies on Excitation and Inhibition in the Retina* (Rockefeller Univ. Press, New York).
16. Knight, B. W., Toyoda, J. & Dodge, F. A. (1970) *J. Gen. Physiol.* **56,** 421–437.
17. Herzog, E. D. (1994) Dissertation (Syracuse University, New York).
18. Passaglia, C. L. (1997) Dissertation (Syracuse University, New York).
19. Barlow, R. B., Chamberlain, S. C. & Levinson, J. Z. (1980) *Science* **210,** 1037–1039.
20. Dodge, F. A., Knight, B. W. & Toyoda, J. I. (1968) *Science* **232,** 1543–1545.
21. Wong, F., Knight, B. W. & Dodge, F. A. (1980) *J. Gen. Physiol.* **76,** 517–537.
22. Fuortes, M. G. F. & Hodgkin, A. L. (1964) *J. Physiol.* **172,** 239–263.
23. Purple, R. L. & Dodge, F. A. (1965) *Cold Spring Harbor Symp. Quant. Biol.* **30,** 529–537.
24. Ratliff, F., Hartline, H. K. & Miller, W. H. (1963) *J. Opt. Soc. Am.* **53,** 110–120.
25. Barlow, R. B. (1969) *J. Gen. Physiol.* **54,** 383–396.
26. Brodie, S. E., Knight, B. W. & Ratliff, F. (1978) *J. Gen. Physiol.* **72,** 167–202.
27. Stevens, C. F. (1964) Dissertation (The Rockefeller University, New York).
28. Smith, T. G., Stell, W. K., Brown, J. E., Freeman, J. A. & Murray, G. C. (1968) *Science* **162,** 456–458.
29. Fohlmeister, J. F., Poppele, R. E. & Purple, R. L. (1977) *J. Gen. Physiol.* **69,** 849–877.
30. Barlow, R. B. & Kaplan, E. H. (1977) *J. Gen. Physiol.* **69,** 203–220.
31. Laughlin, S. B. (1981) in *Comparative Physiology and Evolution of Vision in Invertebrates: Invertebrate Visual Centers and Behavior*, ed. Autrum, H. (Springer, New York), pp. 133–280.
32. Victor, J. D., Shapley, R. M. & Knight, B. W. (1977) *Proc. Natl. Acad. Sci. USA* **74,** 3068–3072.
33. Kaplan, E., Barlow, R. B., Renninger, G. & Purpura, K. (1990) *J. Gen. Physiol.* **96,** 665–685.
34. Batra, R. & Barlow, R. B. (1990) *J. Gen. Physiol.* **95,** 229–244.
35. McFarland, W. N. & Loew, E. R. (1983) *Environ. Biol. Fishes* **8,** 173–183.
36. Passaglia, C. L., Dodge, F. A. & Barlow, R. B. (1995) *Biol. Bull. Woods Hole, Mass.* **189,** 213–215.
37. Loew, E. R. & McFarland, W. N. (1990) in *The Visual System of Fish*, eds. Douglas, R. H. & Djamgoz, M. B. A. (Chapman and Hall, London), pp. 1–43.
38. Passaglia, C. L., McSweeney, M., Stewart, K., Kim, E., Mole, E., Powers, M. & Barlow, R. B. (1997) *Biol. Bull. Woods Hole, Mass.*, in press.
39. Adrian, E. D. (1928) *The Basis of Sensation: The Action of the Sense Organs* (Norton, New York).
40. Hartline, H. K. & Graham, C. H. (1932) *J. Cell Comp. Physiol.* **1,** 227–295.
41. Kiang, N. Y.-S., Watanabe, T., Thomas, E. C. & Clark, L. F. (1965) *Discharge Patterns of Single Fibers in the Cat's Auditory Nerve* (MIT Press, Cambridge, MA).
42. Carr, C. E. & Konishi, M. (1990) *J. Neurosci.* **10,** 3227–3246.
43. Berry, M., Warland, D. & Meister, M. (1997) *Proc. Natl. Acad. Sci. USA* **94,** 5411–5416.
44. Barlow, H. B. (1953) *J. Physiol.* **119,** 69–88.